Hindawi
Journal of Mathematics
Volume 2022, Article ID 5755885, 18 pages
https://doi.org/10.1155/2022/5755885

Research Article

Swarming Computational Procedures for the Coronavirus-Based Mathematical SEIR-NDC Model

Suthep Suantai,[1,2] **Zulqurnain Sabir**,[3] **Muhammad Asif Zahoor Raja**,[4] **and Watcharaporn Cholamjiak**[5]

[1]*Data Science Research Center, Department of Mathematics, Faculty of Science, Chiang Mai University, Chiang Mai 50200, Thailand*
[2]*Research Group in Mathematics and Applied Mathematics, Faculty of Science, Chiang Mai University, Chiang Mai 50200, Thailand*
[3]*Department of Mathematics and Statistics, Hazara University, Mansehra, Pakistan*
[4]*Future Technology Research Center, National Yunlin University of Science and Technology, 123 University Road, Section 3, Douliou, Yunlin 64002, Taiwan*
[5]*School of Science, University of Phayao, Mae Ka, Phayao 56000, Thailand*

Correspondence should be addressed to Watcharaporn Cholamjiak; watcharaporn.ch@up.ac.th

Received 18 July 2022; Accepted 13 October 2022; Published 29 October 2022

Academic Editor: Kolade M. Owolabi

The motive of the current work is related to solving the coronavirus-based mathematical system of susceptible (S), exposed (E), infected (I), recovered (R), overall population (N), civic observation (D), and cumulative performance (C), called as SEIR-NDC. The numerical solutions of the SEIR-NDC model are presented by using the computational framework of artificial neural networks (ANNs) together with the swarming optimization procedures aided with the sequential quadratic programming. The swarming procedure based on the particle swarm optimization (PSO) works as a global search, while the sequential quadratic programming (SQP) is used as a local search algorithm. A merit function is constructed by using the nonlinear dynamics of the SEIR-NDC mathematical system based on its 7 classes, and the optimization of the merit function is performed through the PSOSQP. The numerical expressions of system are accessible with the ANNs using the PSOSQP optimization with 30 variables. The correctness of the stochastic computing scheme performances is verified by using the comparison of the obtained performances of the mathematical SEIR-NDC system and the reference Runge–Kutta scheme. Furthermore, the graphical illustrations of the performance indices, absolute error, and convergence curves are derived to validate the robustness of the proposed ANN-PSOSQP approach for the mathematical SEIR-NDC system.

1. Introduction

The focus of this study is to highlight the health issues along with various diseases that are caused by infections with viruses or bacteria. In addition to disrupting human life, infectious diseases are also seen as a significant threat to economies, businesses, education, and other facets of daily life. One of these viruses, the coronavirus, spread fast throughout the entire world. The transmitting ratio of the coronavirus was very high, and it rapidly spread in the humans from one to another. Millions of people were infected by the coronavirus, which did not discriminate between developed, developing, and underdeveloped nations. After 2.5 years, there are still high number of positive cases reported daily throughout the world. However, the recovery ratio of this virus was so high in its start and now the recovery rate is much higher due to the process of vaccination [1–3]. The symptom of this disease alters with its new shapes, like runny noses, fever, coughs, sore throats, headaches, and respiratory indications (shortness of breath, high fever, bleeding, phlegm, cough, and chest pain) [4–6].

In recent years, one of the main focuses of the researchers is to analyze the outcomes of the coronavirus dynamics by using different effects. Wang [7] presented a mathematical system formulation based on the coronavirus using its applications and capacities. Based on the coronavirus as well as the pregnancy effects, Donders et al. [8] provided the Worldwide Society of Infectious Illness in Gynecology and Obstetrics. Rhodes et al. [9] introduced the coronavirus mathematical model to control the public problems. Khrapov et al. [10] performed the comparative investigations using the mathematical systems of the coronavirus dynamics based on the data of different regions. Jewell et al. [11] presented the potential disruptive impacts using the HIV packages in sub-Saharan Africa based on coronavirus. A coronavirus dynamical system is constructed by Sánchez et al. [12]. Thompson [13] proposed an epidemiological system to consider the significant operators using the coronavirus supervisory interferences. Elsonbaty et al. [14] designed the discrete fractional-order dynamical coronavirus system. Umer et al. [15,16] studied the numerical performances using the swarming as well as heuristic schemes to present the solutions of the coronavirus system. Shikongo et al. [17] presented the fractional-order operator using the principle of quarantine and isolation based on the coronavirus.

Mathematical models appear in a wide range of disciplines, including biology, chemistry, economics, civil and mechanical engineering, and health. According to Side et al. [18] mathematical systems can be used to assess the disease's evolution. Owolabi et al. [19] designed an efficient scheme for the biological stoichiometry model based on tumour dynamics. In another study, they presented the fitted numerical scheme using the HIV model based on the dynamics of cancer-immune system [20]. Some more relevant studies have been presented in [21]. Moreover, few mathematical systems can be accessible analytically, but it is better to perform numerical simulations of the abovementioned systems. Therefore, the computational framework of artificial neural networks (ANNs) together with the swarming optimization procedures aided with the sequential quadratic programming is provided the solve the coronavirus-based mathematical SEIR-NDC system. The swarming procedure based on the particle swarm optimization (PSO) works as a global search, while the sequential quadratic programming (SQP) is used as a local search algorithm. The ANN-based swarming procedures together with PSOSQP have never been applied before to solve the coronavirus-based mathematical SEIR-NDC system. Few famous submissions of the computing stochastic solvers are the prey-predator models [22], delay singular differential models [23, 24], multifractional systems [25–27], periodic singular systems [28,29], nonlinear design of the optics [30], HIV infection system [31], eye surgery models [32, 33], functional singular model [34], mosquito spreading model [35], Thomas–Fermi system [36], smoking model [37], and food chain nonlinear models [38].

The mathematical SEIR-NDC system depends upon seven dynamics, susceptible ($S(y)$), exposed ($E(y)$), infected ($I(y)$), recovered ($R(y)$), overall population ($N(y)$), civic observation ($D(y)$), and growing performance ($C(y)$), shown as [4]

$$\begin{cases} \dfrac{\mathrm{d}S(y)}{dy} = -\psi S(y) - \dfrac{\alpha_0 S(y)E(y)}{N} - \dfrac{\beta I(y)S(y)}{N}, & S_0 = q_1, \\ \dfrac{\mathrm{d}E(y)}{\mathrm{d}y} = \dfrac{\alpha_0 E(y)S(y)}{N} + \dfrac{\beta S(y)I(y)}{N} - (\rho + \psi)E(y), & E_0 = q_2, \\ \dfrac{\mathrm{d}I(y)}{\mathrm{d}y} = \rho E(y) - (\vartheta + \psi)I(y), & I_0 = q_3, \\ \dfrac{\mathrm{d}R(y)}{\mathrm{d}y} = -\psi R(y) + \vartheta I(y), & R_0 = q_4, \\ \dfrac{\mathrm{d}N(y)}{\mathrm{d}y} = -\psi N(y), & N_0 = q_5, \\ \dfrac{\mathrm{d}D(y)}{\mathrm{d}y} = -\phi\ D(y) + \delta\vartheta I(y), & D_0 = q_6, \\ \dfrac{\mathrm{d}C(y)}{\mathrm{d}y} = \rho E(y), & C_0 = q_7, \end{cases} \tag{1}$$

where ψ, ρ, α_0, β, ϑ, ϕ, and δ are the emigration ratio, rate of initial spread, transmission ratio, infected rate, public response, and the severe case. The initial conditions of the model are q_1, q_2, q_3, q_4, q_5, q_6, and q_7. The biological aspects of these initial conditions are well defined in a reported study [19] along with the setting of the parameters such as existence, uniqueness, bounded, and nonnegative of the solution.

The novel topographies of the ANN-PSOSQP are provided as follows:

(i) A neuro swarming computing scheme is presented to solve the coronavirus-based mathematical SEIR-NDC system.

(ii) The swarming procedure based on the PSO is applied as a global search, while the SQP is used as a local search algorithm to solve the coronavirus-based mathematical SEIR-NDC system.

(iii) The stochastic computing scheme is presented efficiently to solve the coronavirus-based mathematical model.

(iv) The comparison of the obtained and reference solutions demonstrates the stochastic approach's correctness.

(v) The absolute error (AE) values are in good measures for the coronavirus-based mathematical SEIR-NDC system, which signifies the exactness of the swarming computing scheme.

(vi) The robustness of the stochastic swarming computing scheme together with PSOSQP is provided by using the statistical performances for multiple trials.

The rest of the paper is organized as follows. Section 2 shows the designed procedures. Section 3 is designed based on the numerical solutions. The concluding comments are presented in the last section.

2. Methodology

The current section provides the stochastic ANN procedure in two steps using the optimization of PSOSQP procedures for solving the mathematical SEIR-NDC system.

(i) A cost function based on the differential SEIR-NDS system is provided.

(ii) Optimization performances of the PSOSQP are provided.

2.1. Modeling: ANNs. The mathematical representations of the SEIR-NDC system are stated using the feed-forward ANNs based on the solutions of 1st derivative as

$$\begin{bmatrix} \widehat{S}(y), \widehat{E}(y), \\ \widehat{I}(y), \widehat{R}(y), \\ \widehat{N}(y), \widehat{D}(y), \\ \widehat{C}(y) \end{bmatrix} = \begin{bmatrix} \sum_{n=1}^{m} b_{S,n} T\left(w_{S,n} y + u_{S,n}\right), \sum_{n=1}^{m} b_{E,n} T\left(w_{E,n} y + u_{E,n}\right), \\ \sum_{n=1}^{m} b_{I,n} T\left(w_{I,n} y + u_{I,n}\right), \sum_{n=1}^{m} b_{R,n} T\left(w_{R,n} y + u_{R,n}\right), \\ \sum_{n=1}^{m} b_{N,n} T\left(w_{N,n} y + u_{N,n}\right), \sum_{n=1}^{m} b_{D,n} T\left(w_{D,n} y + u_{D,n}\right), \\ \sum_{n=1}^{m} b_{C,n} T\left(w_{C,n} y + u_{C,n}\right) \end{bmatrix}, \tag{2}$$

$$\begin{bmatrix} \frac{\mathrm{d}}{\mathrm{d}y}\widehat{S}(y), \frac{\mathrm{d}}{\mathrm{d}y}\widehat{E}(y), \\ \frac{\mathrm{d}}{\mathrm{d}y}\widehat{I}(y), \frac{\mathrm{d}}{\mathrm{d}y}\widehat{R}(y), \\ \frac{\mathrm{d}}{\mathrm{d}y}\widehat{N}(y), \frac{\mathrm{d}}{\mathrm{d}y}\widehat{D}(y), \\ \frac{\mathrm{d}}{\mathrm{d}y}\widehat{C}(y) \end{bmatrix} = \begin{bmatrix} \sum_{n=1}^{m} b_{S,n} \frac{\mathrm{d}}{\mathrm{d}y} T\left(w_{S,n} y + u_{S,n}\right), \sum_{n=1}^{m} b_{E,n} \frac{\mathrm{d}}{\mathrm{d}y} T\left(w_{E,n} y + u_{E,n}\right), \\ \sum_{n=1}^{m} b_{I,n} \frac{\mathrm{d}}{\mathrm{d}y} T\left(w_{I,k} y + u_{I,k}\right), \sum_{n=1}^{m} b_{R,n} \frac{\mathrm{d}}{\mathrm{d}y} T\left(w_{R,n} y + u_{R,n}\right), \\ \sum_{n=1}^{m} b_{N,n} \frac{\mathrm{d}}{\mathrm{d}y} T\left(w_{N,k} y + u_{N,k}\right), \sum_{n=1}^{m} b_{D,n} \frac{\mathrm{d}}{\mathrm{d}y} T\left(w_{D,n} y + u_{D,n}\right), \\ \sum_{n=1}^{m} b_{C,n} \frac{\mathrm{d}}{\mathrm{d}y} T\left(w_{C,k} y + u_{C,k}\right) \end{bmatrix}, \tag{3}$$

where m shows the number of neurons, T is the activation function, and the first derivative is used due to the nature of the 1st order SEIR-NDC system. The unidentified weights are represented by $\mathbf{W}$ and written as $\mathbf{W} = \begin{bmatrix} \mathbf{W}_S \\ \mathbf{W}_E \\ \mathbf{W}_I \\ \mathbf{W}_R \\ \mathbf{W}_N \\ \mathbf{W}_D \\ \mathbf{W}_C \end{bmatrix}^t$, where $\mathbf{W}_S = \begin{bmatrix} \mathbf{b}_S \\ \mathbf{w}_S \\ \mathbf{u}_S \end{bmatrix}^t$, $\mathbf{W}_E = \begin{bmatrix} \mathbf{b}_E \\ \mathbf{w}_E \\ \mathbf{u}_E \end{bmatrix}^t$, $\mathbf{W}_I = \begin{bmatrix} \mathbf{b}_I \\ \mathbf{w}_I \\ \mathbf{u}_I \end{bmatrix}^t$, $\mathbf{W}_R = \begin{bmatrix} \mathbf{b}_R \\ \mathbf{w}_R \\ \mathbf{u}_R \end{bmatrix}^t$, $\mathbf{W}_N = \begin{bmatrix} \mathbf{b}_N \\ \mathbf{w}_N \\ \mathbf{u}_N \end{bmatrix}^t$, $\mathbf{W}_D = \begin{bmatrix} \mathbf{b}_D \\ \mathbf{w}_D \\ \mathbf{u}_D \end{bmatrix}^t$, and $\mathbf{W}_C = \begin{bmatrix} \mathbf{b}_C \\ \mathbf{w}_C \\ \mathbf{u}_C \end{bmatrix}^t$.

$\mathbf{b}_S = [b_{S,1}, b_{S,2}, \ldots, b_{S,m}]$, $\mathbf{b}_E = [b_{E,1}, b_{E,2}, \ldots, b_{E,m}]$, $\mathbf{b}_I = [b_{I,1}, b_{I,2}, \ldots, b_{I,m}]$, $\mathbf{b}_R = [b_{R,1}, b_{R,2}, \ldots, b_{R,m}]$, $\mathbf{b}_N = [b_{N,1}, b_{N,2}, \ldots, b_{N,m}]$, $\mathbf{b}_D = [b_{D,1}, b_{D,2}, \ldots, b_{D,m}]$, $\mathbf{b}_C = [b_{C,1}, b_{C,2}, \ldots, b_{C,m}]$, $\mathbf{w}_S = [w_{S,1}, w_{S,2}, \ldots, w_{S,m}]$, $\mathbf{w}_E = [w_{E,1}, w_{E,2}, \ldots, w_{E,m}]$, $\mathbf{w}_I = [w_{I,1}, w_{I,2}, \ldots, w_{I,m}]$, $\mathbf{w}_R = [w_{R,1}, w_{R,2}, \ldots, w_{R,m}]$, $\mathbf{w}_N = [w_{N,1}, w_{N,2}, \ldots, w_{N,m}]$, $\mathbf{w}_D = [w_{D,1}, w_{D,2}, \ldots, w_{D,m}]$, $\mathbf{w}_C = [w_{C,1}, w_{C,2}, \ldots, w_{C,m}]$, $\mathbf{u}_S = [u_{S,1}, u_{S,2}, \ldots, u_{S,m}]$, $\mathbf{u}_E = [u_{E,1}, u_{E,2}, \ldots, u_{E,m}]$, $\mathbf{u}_I = [u_{I,1}, u_{I,2}, \ldots, u_{I,m}]$, $\mathbf{u}_R = [u_{R,1}, u_{R,2}, \ldots, u_{R,m}]$, $\mathbf{u}_N = [u_{N,1}, u_{N,2}, \ldots, u_{N,m}]$, $\mathbf{u}_D = [u_{D,1}, u_{D,2}, \ldots, u_{D,m}]$, $\mathbf{u}_C = [u_{C,1}, u_{C,2}, \ldots, u_{C,m}]$.

A log-sigmoid activation function (LSAF) is used in this work, and the mathematical formulation of LSAF is provided as $T(y) = 1/1 + e^{-y}$. Put the values of LSAF in equation (2), and then first-order derivative has been performed, which is shown in the following equation:

$$\begin{bmatrix} \widehat{S}(y), \widehat{E}(y), \widehat{I}(y), \\ \widehat{R}(y), \widehat{N}(y), \widehat{D}(y), \\ \widehat{C}(y) \end{bmatrix} = \begin{bmatrix} \sum_{n=1}^{m} \frac{b_{S,n}}{1+e^{-(w_{S,n}y+u_{S,n})}}, \sum_{n=1}^{m} \frac{b_{E,n}}{1+e^{-(w_{E,n}y+u_{E,n})}}, \sum_{n=1}^{m} \frac{b_{I,n}}{1+e^{-(w_{I,n}y+u_{I,n})}} \\ \sum_{n=1}^{m} \frac{b_{R,n}}{1+e^{-(w_{R,n}y+u_{R,n})}}, \sum_{n=1}^{m} \frac{b_{N,n}}{1+e^{-(w_{N,n}y+u_{N,n})}}, \sum_{n=1}^{m} \frac{b_{D,n}}{1+e^{-(w_{D,n}y+u_{D,n})}}, \\ \sum_{n=1}^{m} \frac{b_{C,n}}{1+e^{-(w_{C,n}y+u_{C,n})}} \end{bmatrix},$$

$$\begin{bmatrix} \frac{\mathrm{d}}{\mathrm{d}y}\widehat{S}(y), \frac{\mathrm{d}}{\mathrm{d}y}\widehat{E}(y), \\ \frac{\mathrm{d}}{\mathrm{d}y}\widehat{I}(y), \frac{\mathrm{d}}{\mathrm{d}y}\widehat{R}(y), \\ \frac{\mathrm{d}}{\mathrm{d}y}\widehat{N}(y), \frac{\mathrm{d}}{\mathrm{d}y}\widehat{D}(y), \\ \frac{\mathrm{d}}{\mathrm{d}y}\widehat{C}(y) \end{bmatrix} = \begin{bmatrix} \sum_{n=1}^{m} \frac{w_{S,n}b_{S,n}e^{-(w_{S,n}y+u_{S,n})}}{\left(1+e^{-(w_{S,k}\aleph+p_{S,k})}\right)^2}, \sum_{n=1}^{m} \frac{w_{E,n}b_{E,n}e^{-(w_{E,n}y+u_{E,n})}}{\left(1+e^{-(w_{E,n}y+u_{E,n})}\right)^2}, \\ \sum_{n=1}^{m} \frac{w_{I,n}b_{I,n}e^{-(w_{I,n}y+u_{I,n})}}{\left(1+e^{-(w_{I,n}y+u_{I,n})}\right)^2}, \sum_{n=1}^{m} \frac{w_{R,n}b_{R,n}e^{-(w_{R,n}y+u_{R,n})}}{\left(1+e^{-(w_{R,n}y+u_{R,n})}\right)^2}, \\ \sum_{n=1}^{m} \frac{w_{N,n}b_{N,n}e^{-(w_{N,n}y+u_{N,n})}}{\left(1+e^{-(w_{N,n}y+u_{N,n})}\right)^2}, \sum_{n=1}^{m} \frac{w_{D,n}b_{D,n}e^{-(w_{D,n}y+u_{D,m})}}{\left(1+e^{-(w_{D,n}y+u_{D,m})}\right)^2}, \\ \sum_{n=1}^{m} \frac{w_{C,n}b_{C,n}e^{-(w_{C,n}y+u_{C,n})}}{\left(1+e^{-(w_{C,n}y+u_{C,n})}\right)^2} \end{bmatrix}. \tag{4}$$

The cost function is provided as

$$E_C = E_{C-1} + E_{E-2} + E_{E-3} + E_{E-4} + E_{E-5} + E_{E-6} + E_{F-7} + E_{F-8}, \tag{5}$$

$$E_{C-1} = \frac{1}{N}\sum_{n=1}^{N}\left(\frac{\mathrm{d}\widehat{S}}{\mathrm{d}y_n} + \frac{\alpha_0\widehat{S}_n\widehat{E}_n}{N} + \frac{\beta\widehat{I}_n\widehat{S}_n}{N} + \psi\widehat{S}_k\right)^2, \tag{6}$$

$$E_{C-2} = \frac{1}{N}\sum_{n=1}^{N}\left(\frac{\mathrm{d}\widehat{E}}{\mathrm{d}y_n} - \frac{\alpha_0\widehat{S}_n\widehat{E}_n}{N} - \frac{\beta\widehat{I}_n\widehat{S}_n}{N} + \psi\widehat{E}_n + \rho\widehat{E}_n\right)^2, \tag{7}$$

$$E_{C-3} = \frac{1}{N}\sum_{n=1}^{N}\left(\frac{\mathrm{d}\widehat{I}}{\mathrm{d}y_n} + \vartheta\widehat{I}_n + \psi\widehat{I}_n - \rho\widehat{E}_n\right)^2, \tag{8}$$

$$E_{C-4} = \frac{1}{N}\sum_{n=1}^{N}\left(\frac{\mathrm{d}\widehat{R}}{\mathrm{d}y_n} - \vartheta\widehat{I}_n + \psi\widehat{R}_n\right)^2, \tag{9}$$

$$E_{C-5} = \frac{1}{N}\sum_{n=1}^{N}\left(\frac{\mathrm{d}\widehat{N}}{\mathrm{d}y_n} + \psi\widehat{N}_n\right)^2, \tag{10}$$

$$E_{C-6} = \frac{1}{N}\sum_{n=1}^{N}\left(\frac{\mathrm{d}\widehat{D}}{\mathrm{d}y_n} + \phi\widehat{D}_n - \delta\vartheta\widehat{I}_n\right)^2, \tag{11}$$

$$E_{C-7} = \frac{1}{N}\sum_{n=1}^{N}\left(\frac{\mathrm{d}\widehat{C}}{\mathrm{d}y_n} - \rho\widehat{E}_n\right)^2, \tag{12}$$

$$E_{C-8} = \frac{1}{7}\Big(\left(\widehat{S}_0 - q_1\right)^2 + \left(\widehat{E}_0 - q_2\right)^2 + \left(\widehat{I}_0 - q_3\right)^2 + \left(\widehat{R}_0 - q_4\right)^2 + \left(\widehat{N}_0 - q_5\right)^2 + \left(\widehat{D}_0 - q_6\right)^2 + \left(\widehat{C}_0 - q_7\right)^2\Big), \tag{13}$$

where $Nh = 1$, $\widehat{E}_n = \widehat{E}(y_n)$, $\widehat{D}_n = \widehat{D}(y_n), \widehat{S}_n = \widehat{S}(y_n), \widehat{N}_n = \widehat{N}(y_n), \widehat{I}_n = \widehat{I}(y_n), \widehat{R}_n = \widehat{R}(y_n), \widehat{C}_n = \widehat{C}(y_n)$, and $y_n = nh$. The proposed results are $\widehat{S}_n = \widehat{S}(y_n), \widehat{I}_n = \widehat{I}(y_n), \widehat{E}_n = \widehat{E}(y_n), \widehat{R}_n = \widehat{R}(y_n), \widehat{N}_n = \widehat{N}(y_n), \widehat{D}_n = \widehat{D}(y_n)$, and $\widehat{C}_n = \widehat{C}(y_n)$. Moreover, $E_{C-1}, E_{C-2}, E_{C-3}, E_{C-4}, E_{C-5}, E_{C-6}, E_{C-7}$, and E_{C-8} are the cost functions using SEIR-NDC system and its initial conditions, respectively.

2.2. Optimization: PSOSQP. The optimization performances based on the swarming procedures based on the PSO along with the SQP procedures are presented using the mathematical SEIR-NDC system.

The global search swarming procedure PSO is used as an alteration of the genetic algorithm. PSO was discovered in the 7th decade of the 19th century. PSO provides best solution performance to solve the stiff and nonstiff natured problems. Recently, PSO has been applied in widespread applications, such as mixed-variable optimization systems [39], solar energy systems [40], plant diseases diagnosis [41], feature selection in cataloging [42], organizing the single, double, and three diode photovoltaic systems [43], particle filter noise reduction in mechanical fault diagnosis [44], big data excavation of hot subjects about recycled water based on the microblog [45], 2nd order functional singular differential system [34], and green coal production problem [46].

The efficient and rapid performances of the results have been obtained through the hybridization of the swarming optimization schemes with the local search method. Hence, SQP is used as a local search scheme with the hybridization of PSO. The local search PSO approach is used by taking the initial PSO input to perform the quick results. In recent decades, PSO has been functional in the variety of applications, like optimal power flow problem [47], dynamic economic dispatch [48], constrained nonlinear control allocation with singularity avoidance [49], four-level integrated supply chain with the aim of determining the optimum stockpile and period length [50], and multivariate regression based on the fuel cell using the electric vehicle [51]. The present investigations are related to indicate the numerical performances based on the mathematical system using the PSOSQP. The stochastic PSOSQP procedure for the mathematical SEIR-NDC system is provided in Figure 1. The descriptions of the PSO and SQP are tabulated in Table 1.

2.3. Statistical Performance. The current section presents the statistical representations of the mean square error (MSE), Theil's inequality coefficient (TIC), and semi-interquartile range (SIR) for mathematical SEIR-NDC system. The statistical performances are used to check the reliability of the stochastic scheme. The mathematical form of these operators is given as

$$\begin{bmatrix} \mathrm{MSE}_S, \mathrm{MSE}_E, \mathrm{MSE}_I, \\ \mathrm{MSE}_R, \mathrm{MSE}_N, \mathrm{MSE}_D, \\ \mathrm{MSE}_C \end{bmatrix} = \begin{bmatrix} \sum_{j=1}^{n}\left(S_j - \widehat{S}_j\right)^2, \sum_{j=1}^{n}\left(E_j - \widehat{E}_j\right)^2, \sum_{j=1}^{n}\left(I_j - \widehat{I}_j\right)^2, \\ \sum_{j=1}^{n}\left(R_j - \widehat{R}_j\right)^2, \sum_{j=1}^{n}\left(N_j - \widehat{N}_j\right)^2, \sum_{j=1}^{n}\left(D_j - \widehat{D}_j\right)^2, \\ \sum_{j=1}^{n}\left(C_j - \widehat{C}_j\right)^2 \end{bmatrix} A,$$

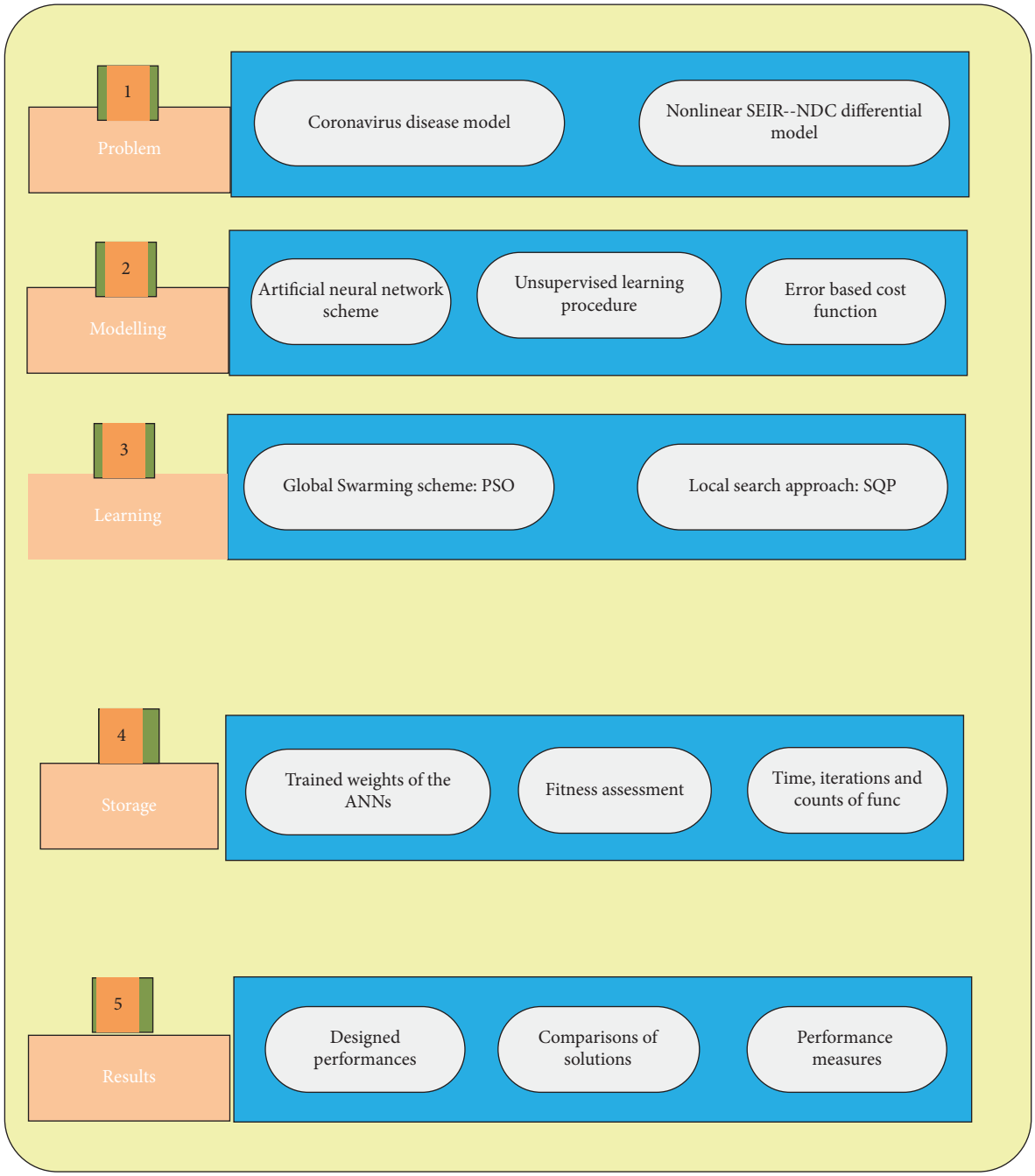

Figure 1: Stochastic PSOSQP scheme for the mathematical SEIR-NDC system.

Table 1: Optimization PSOSQP scheme for the mathematical SEIR-NDC system.

PSO procedure

[Inputs]: The chromosomes are presented as $W = [\mathbf{bw}, \mathbf{u}]$.

[Population]: Chromosome sets are presented as

$$\mathbf{W} = \begin{bmatrix} \mathbf{W}_S \\ \mathbf{W}_E \\ \mathbf{W}_I \\ \mathbf{W}_R \\ \mathbf{W}_N \\ \mathbf{W}_D \\ \mathbf{W}_C \end{bmatrix}^t, \text{ where } \mathbf{W}_S = \begin{bmatrix} \mathbf{b}_S \\ \mathbf{w}_S \\ \mathbf{u}_S \end{bmatrix}^t, \mathbf{W}_E = \begin{bmatrix} \mathbf{b}_E \\ \mathbf{w}_E \\ \mathbf{u}_E \end{bmatrix}^t, \mathbf{W}_I = \begin{bmatrix} \mathbf{b}_I \\ \mathbf{w}_I \\ \mathbf{u}_I \end{bmatrix}^t, \mathbf{W}_R = \begin{bmatrix} \mathbf{b}_R \\ \mathbf{w}_R \\ \mathbf{u}_R \end{bmatrix}^t, \mathbf{W}_N = \begin{bmatrix} \mathbf{b}_N \\ \mathbf{w}_N \\ \mathbf{u}_N \end{bmatrix}^t, \mathbf{W}_D = \begin{bmatrix} \mathbf{b}_D \\ \mathbf{w}_D \\ \mathbf{u}_D \end{bmatrix}^t \text{ and } \mathbf{W}_C = \begin{bmatrix} \mathbf{b}_C \\ \mathbf{w}_C \\ \mathbf{u}_C \end{bmatrix}^t.$$

[Output]: Best PSO weights are denoted as WBPSO.

Initialization: The collection of chromosomes represents the WBPSO values.

[Fitness Valuation]: Adjust the fitness (E_C) using the population [P] through systems 4–12.

(i) [Terminating Standards]: Terminate the process, when the below criteria meets, [TolCon = 10–19], [Generations = 120], [E_C = 10–19], [TolFun = 10–21], [StallLimit = 110], and [Size of population = 210].

Move to [storage].

[Ranking]: WBPSO shows the population rank for E_C.

[Storage]: [WBPSO], E_C, [iterations], [time], and [Counts of function] for PSO.

[PSO] process ends.

[SQP] process starts.

[Inputs]: WBPSO.

[Output]: WPSOSQP represents the best values of the weights.

[Initialize]: WPSOSQP, Iterations and Assignments.

[Stopping rules]: [Iterations = 170], [E_C = 10–20], [Max-Fun-Evals = 170000] and [TolFun = 10–19], [Tol-X = 10–22].

[FIT Calculation]: Compute [WBPSO] and E_C through equations (5)–(13).

[Amendments]: Regulate [fmincon] for SQP, E_C to perform the 'W' for equations (5)–(13).

[Store]: Transform WBPSO,nt.

[SQP] process ends.

$$\begin{bmatrix} \mathrm{TIC}_S, \mathrm{TIC}_E, \mathrm{TIC}_I, \\ \mathrm{TIC}_R, \mathrm{TIC}_N, \mathrm{TIC}_D, \\ \mathrm{TIC}_C \end{bmatrix} = \begin{bmatrix} \dfrac{\sqrt{(1/n)\sum_{j=1}^{n}\left(S_j - \widehat{S}_j\right)^2}}{\left(\sqrt{(1/n)\sum_{j=1}^{n} S_j^2} + \sqrt{(1/n)\sum_{j=1}^{n} \widehat{S}_j^2}\right)}, \dfrac{\sqrt{(1/n)\sum_{j=1}^{n}\left(E_j - \widehat{E}_j\right)^2}}{\left(\sqrt{(1/n)\sum_{j=1}^{n} E_j^2} + \sqrt{(1/n)\sum_{j=1}^{n} \widehat{E}_j^2}\right)}, \\ \dfrac{\sqrt{(1/n)\sum_{j=1}^{n}\left(I_j - \widehat{I}_j\right)^2}}{\left(\sqrt{(1/n)\sum_{j=1}^{n} I_j^2} + \sqrt{(1/n)\sum_{j=1}^{n} \widehat{I}_j^2}\right)}, \dfrac{\sqrt{(1/n)\sum_{j=1}^{n}\left(R_j - \widehat{R}_j\right)^2}}{\left(\sqrt{(1/n)\sum_{j=1}^{n} R_j^2} + \sqrt{(1/n)\sum_{j=1}^{n} \widehat{R}_k^2}\right)}, \\ \dfrac{\sqrt{(1/n)\sum_{j=1}^{n}\left(N_j - \widehat{N}_j\right)^2}}{\left(\sqrt{(1/n)\sum_{j=1}^{n} N_j^2} + \sqrt{(1/n)\sum_{j=1}^{n} \widehat{N}_j^2}\right)}, \dfrac{\sqrt{(1/n)\sum_{j=1}^{n}\left(D_j - \widehat{D}_j\right)^2}}{\left(\sqrt{(1/n)\sum_{j=1}^{n} \widehat{D}_j^2} + \sqrt{(1/n)\sum_{j=1}^{n} \widehat{D}_j^2}\right)}, \\ \dfrac{\sqrt{(1/n)\sum_{j=1}^{n}\left(C_k - \widehat{C}_k\right)^2}}{\left(\sqrt{(1/n)\sum_{j=1}^{n} \widehat{C}_j^2} + \sqrt{(1/n)\sum_{j=1}^{n} \widehat{C}_j^2}\right)} \end{bmatrix}, \tag{14}$$

$$\mathrm{SIR} = -0.5\left(1^{st}\mathrm{Quartile} - 3^{r\,d}\mathrm{Quartile}\right),$$

where $S(y)$, $E(y)$, $I(y)$, $R(y)$, $N(y)$, $D(y)$, and $C(y)$ indicate the reference solutions, while the hat terms present the proposed solutions that have been obtained by using the proposed scheme.

3. Result Performances

The current section shows the numerical performances of the results for the mathematical SEIR-NDC system by applying the proposed ANN-PSOSQP procedure.

3.1. Mathematical SEIR-NDC System. The updated form of the mathematical SEIR-NDC system is provided by adjusting the appropriate parameter performances, written as

$$\begin{cases} \frac{\mathrm{d}S(y)}{\mathrm{d}y} = -\frac{0.5S(y)E(y)}{N} - \frac{0.6IS(y)}{N} - 0.0205S(y), & S_0 = 0.9, \\ \frac{\mathrm{d}E(y)}{dy} = \frac{0.5ES(y)}{N} + \frac{0.6IS(y)}{N} - 0.3505E(y), & E_0 = 0.1, \\ \frac{\mathrm{d}I(y)}{\mathrm{d}y} = \frac{1}{3}E(y) - 0.225I(y), & I_0 = 0, \\ \frac{\mathrm{d}R(y)}{\mathrm{d}y} = -0.025R(y) + \frac{1}{5}I(y), & R_0 = 0, \\ \frac{\mathrm{d}N(y)}{\mathrm{d}y} = -0.0205N(y), & N_0 = 14, \\ \frac{\mathrm{d}D(y)}{\mathrm{d}y} = -\frac{1}{11.2}D(y) + 0.04I(y), & D_0 = 0, \\ \frac{\mathrm{d}C(y)}{\mathrm{d}y} = \frac{1}{3}E(y), & C_0 = 0. \end{cases} \tag{15}$$

The cost function is designed in terms of mean square error, which is based on the differential SEIR-NDC system given in equation (1) by keeping the methodology of equation (5) shown as

$$E_C = \frac{1}{N}\sum_{n=1}^{N}\left(\begin{array}{c} \left[\frac{\mathrm{d}\widehat{S}}{\mathrm{d}y_n} + \frac{0.6\widehat{S}_n\widehat{I}_n}{N} + \frac{0.5\widehat{S}_n\widehat{E}_n}{N} + 0.0205\widehat{S}_k\right]^2 + \\ \left[\frac{\mathrm{d}\widehat{E}}{\mathrm{d}y_n} - \frac{0.6\widehat{S}_n\widehat{I}_n}{N} + 0.3505\widehat{E}_n - \frac{0.5\widehat{E}_n\widehat{S}_n}{N}\right]^2 + \\ \left[\frac{\mathrm{d}\widehat{I}}{\mathrm{d}y_n} - 0.333\widehat{E}_n + 0.225\widehat{I}_n\right]^2 + \left[\frac{\mathrm{d}\widehat{R}}{\mathrm{d}y_n} - 0.2\widehat{I}_n + 0.025\widehat{R}_n\right]^2 \\ \left[\frac{\mathrm{d}\widehat{N}}{\mathrm{d}y_n} + 0.0205\widehat{N}_n\right]^2 + \left[\frac{\mathrm{d}\widehat{D}}{\mathrm{d}y_n} + \frac{1}{11.2}\widehat{D}_n - 0.04\widehat{I}_n\right]^2 + \left[\frac{\mathrm{d}\widehat{C}}{\mathrm{d}y_n} - 0.33\widehat{E}_n\right]^2 \end{array}\right) \tag{16}$$

$$+\frac{1}{7}\left(\left(\widehat{S}_0 - 0.9\right)^2 + \left(\widehat{E}_0 - 0.1\right)^2 + \left(\widehat{I}_0\right)^2 + \left(\widehat{R}_0\right)^2 + \left(\widehat{N}_0 - 14\right)^2 + \left(\widehat{D}_0\right)^2 + \left(\widehat{C}_0\right)^2\right).$$

The solutions of the mathematical model are obtained through the optimization-based PSOSQP for 30 runs together with 10 neurons and 30 variables. The best values of the weights using the ANNs along with the optimization

procedures of PSOSQP are illustrated in Figure 2. These weight vectors are capable to achieve the proposed outcomes based on the mathematical SEIR-NDC system. The obtained solutions are presented as

$$\begin{aligned}\widehat{S}(y) = {} & \frac{-0.2642}{1+e^{-(-0.3453y-2.7523)}} - \frac{1.1108}{1+e^{-(-0.0416y-3.3393)}} + \frac{1.1575}{1+e^{-(-0.0138y-1.4023)}} - \frac{2.7090}{1+e^{-(0.0464y-4.5616)}} \\ & - \frac{1.6702}{1+e^{-(-0.3570y-4.4423)}} - \frac{2.6603}{1+e^{-(-0.0283y-4.2419)}} + \frac{1.7547}{1+e^{-(-0.029y-0.3310)}} + \frac{0.0091}{1+e^{-(-2.652y-3.6896)}} \\ & - \frac{1.5576}{1+e^{-(-0.3541y-3.7727)}} + \frac{0.7427}{1+e^{-(0.3299y-1.7304)}},\end{aligned} \tag{17}$$

$$\begin{aligned}\widehat{E}(y) = {} & \frac{-0.6539}{1+e^{-(0.4382y-2.7725)}} + \frac{0.7297}{1+e^{-(0.2924y-0.8677)}} + \frac{0.2659}{1+e^{-(0.0822y-2.7119)}} - \frac{0.1812}{1+e^{-(0.1846y-2.6274)}} \\ & - \frac{0.6085}{1+e^{-(-0.4121y-3.4072)}} - \frac{0.1400}{1+e^{-(-1.906y-4.1492)}} - \frac{0.3712}{1+e^{-(0.3892y-2.6735)}} + \frac{0.6967}{1+e^{-(-0.186y-1.9214)}} \\ & + \frac{0.1559}{1+e^{-(-2.6372y-4.3152}} - \frac{0.2011}{1+e^{-(0.9194y+0.5422)}},\end{aligned} \tag{18}$$

$$\begin{aligned}\widehat{I}(y) = {} & \frac{-0.0574}{1+e^{-(1.2464y-0.8872)}} + \frac{0.2187}{1+e^{-(-1.3408y+0.2756)}} + \frac{0.0617}{1+e^{-(0.4227y-1.7866}} - \frac{0.2980}{1+e^{-(-1.2379y+0.2365)}} \\ & - \frac{0.0133}{1+e^{-(-1.605y+1.2206)}} - \frac{0.4663}{1+e^{-(-0.4652y+0.2808)}} + \frac{0.7394}{1+e^{-(-0.400y-0.5017)}} + \frac{0.6493}{1+e^{-(0.4898y+1.4072)}} \\ & - \frac{0.7298}{1+e^{-(-0.0279y+0.0603)}} - \frac{0.2452}{1+e^{-(0.3425y-0.3986)}},\end{aligned} \tag{19}$$

$$\begin{aligned}\widehat{R}(y) = {} & \frac{0.1559}{1+e^{-(-0.0877y+0.1975)}} + \frac{1.2832}{1+e^{-(0.0576y-0.8472)}} + \frac{1.0399}{1+e^{-(-0.065y-0.8056)}} - \frac{1.2887}{1+e^{-(-0.574y+0.1095)}} \\ & - \frac{1.2887}{1+e^{-(-0.5745y+0.1095)}} + \frac{2.0675}{1+e^{-((0.0278y-0.8404)}} + \frac{0.6345}{1+e^{-(0.2984y-1.3477)}} - \frac{0.8935}{1+e^{-(0.4460y+0.1236)}} \\ & + \frac{0.1527}{1+e^{-(0.7777y+0.88888)}} - \frac{1.0334}{1+e^{-(0.6031y-0.1048)}},\end{aligned} \tag{20}$$

$$\begin{aligned}\widehat{N}(y) = {} & \frac{-0.3884}{1+e^{-(0.6558y-1.2335)}} + \frac{3.5190}{1+e^{-(-0.6532y+1.0132)}} - \frac{1.6826}{1+e^{-(1.4236y-1.3726)}} + \frac{1.7911}{1+e^{-(-1.3963y-1.700)}} \\ & + \frac{4.0516}{1+e^{-(-0.1159y+2.0362)}} + \frac{5.3651}{1+e^{-(0.5579y+2.6055)}} + \frac{0.8774}{1+e^{-(1.6682y-1.5831)}} - \frac{0.1755}{1+e^{-(0.3419y-0.5896)}} \\ & + \frac{4.7250}{1+e^{-(0.4341y+0.3914)}} + \frac{0.7509}{1+e^{-(1.1986y-2.0756)}},\end{aligned} \tag{21}$$

$$\begin{aligned}\widehat{D}(y) = {} & \frac{0.0346}{1+e^{-(0.4044y+0.1385)}} + \frac{0.0369}{1+e^{-(-0.6492y-1.3941)}} + \frac{0.0252}{1+e^{-(0.6736y-3.6858)}} - \frac{0.1954}{1+e^{-(-0.0098y-0.552)}} \\ & - \frac{0.4620}{1+e^{-(-0.3519y-1.7583)}} - \frac{0.0031}{1+e^{-(2.5703y+1.1318)}} - \frac{0.2087}{1+e^{-(0.4861y+0.7123)}} + \frac{0.4475}{1+e^{-(0.1428y+1.0332)}} \\ & - \frac{0.3525}{1+e^{-(0.1370y-1.0306)}} + \frac{0.0485}{1+e^{-(0.0037y-0.5402)}},\end{aligned} \tag{22}$$

$$\begin{aligned}\widehat{C}(y) = {} & \frac{0.4009}{1+e^{-(-0.9719y-1.4703)}} - \frac{0.0180}{1+e^{-(1.8583y+1.2249)}} - \frac{0.0480}{1+e^{-(-1.3170y-1.1695)}} - \frac{0.2347}{1+e^{-(0.5107y-0.4262)}} \\ & - \frac{0.2811}{1+e^{-(0.3620y-0.3718)}} - \frac{0.2071}{1+e^{-(-0.1348y+0.1319)}} + \frac{1.23280}{1+e^{-(0.2702y+0.8495)}} - \frac{1.2549}{1+e^{-(-0.0358y-0.3046)}} \\ & - \frac{0.5549}{1+e^{-(-0.4663y-1.5261)}} + \frac{0.1058}{1+e^{-(-0.7565y-0.8043)}}.\end{aligned} \tag{23}$$

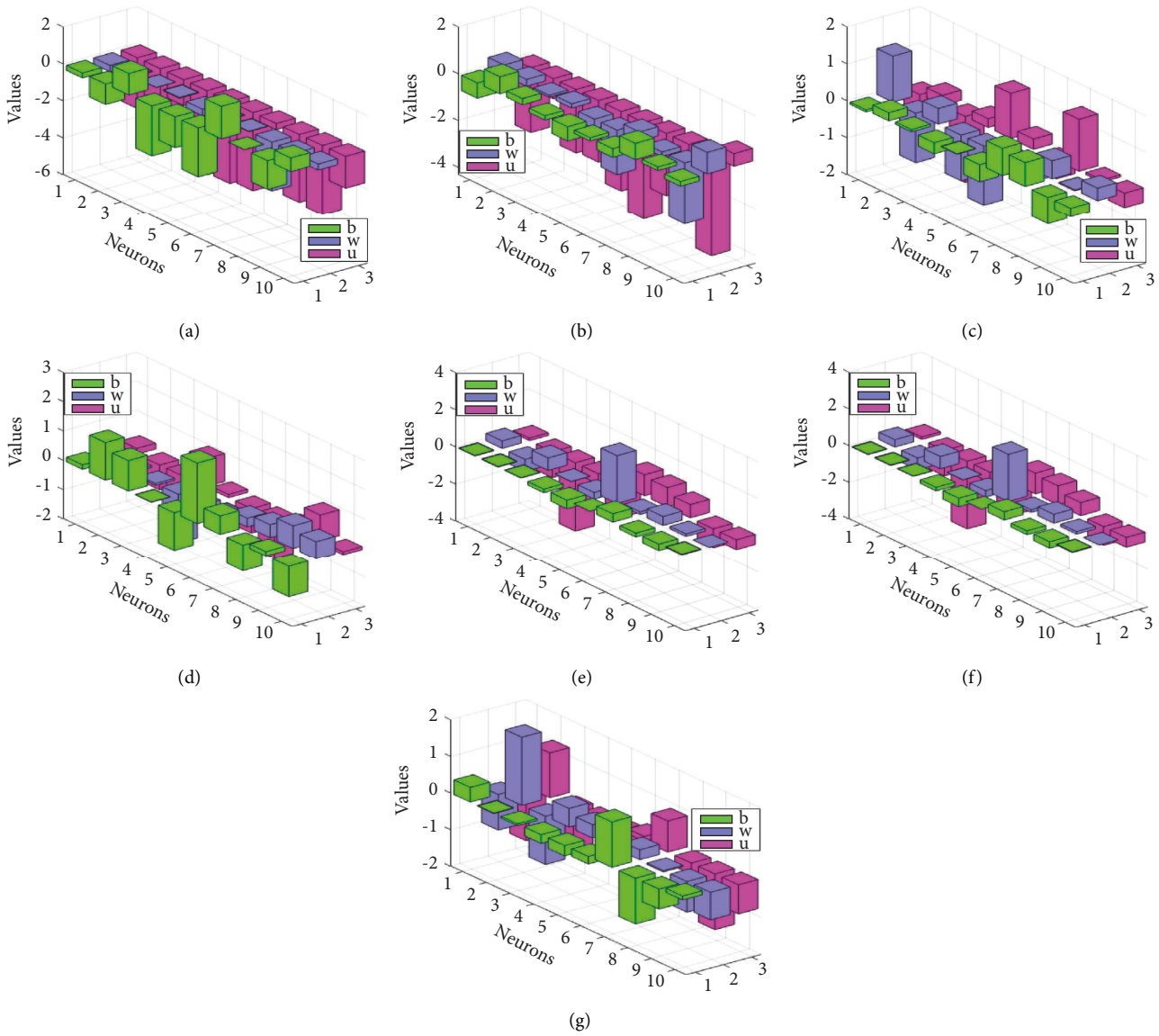

FIGURE 2: Weights for solving the mathematical SEIR-NDC system. (a) Weights: $\widehat{S}(y)$. (b) Weights: $\widehat{E}(y)$. (c) Weights: $\widehat{I}(y)$. (d) Weights: $\widehat{R}(y)$. (e) Weights: $\widehat{N}(y)$. (f) Weights: $\widehat{D}(y)$. (g) Weights: $\widehat{C}(y)$.

The above equations are given to evaluate the outputs of the SEIR-NDC model by operating the ANNs and PSOSQP. The achieved outcomes are illustrated in Figures 2–4 using 10 neurons and 30 variables. Figures 2(a)–2(g) represent the optimal weight vectors for the model. These optimal weights have been obtained by using equations (17)–(23). The solutions have been obtained by using these weight vectors. Figures 3(a)–3(g) show the proposed, mean, and best result comparison for the mathematical SEIR-NDC system. The proposed results have been obtained by using the designed ANN procedure along with the computing swarming scheme, and the best solutions indicate the ideal solutions, while the mean solutions have been achieved by using the mean performances. The matching of the mean, obtained, and best results indicates the exactness of the designed ANN procedure along with the computing swarming scheme. Figure 4 presents the AE performances based on the mean and the best solutions for the mathematical SEIR-NDC system. It is shown that the best outcomes of the AE to solve the respective categories of the model are 10^{-05}–10^{-06}, 10^{-05}–10^{-07}, 10^{-03}–10^{-05}, 10^{-04}–10^{-07}, 10^{-07}–10^{-08}, 10^{-05}–10^{-08}, and 10^{-06}–10^{-09} for each category of the model. The performances based on the mean for the respective categories of the model are presented as 10^{-04}–10^{-05}, 10^{-03}–10^{-05}, 10^{-03}–10^{-04}, 10^{-04}–10^{-05}, 10^{-05}–10^{-06}, 10^{-04}–10^{-06}, and 10^{-05}–10^{-06} for each dynamics of the model. These observed AE values show the accurateness of ANN-PSOSQP procedure for SEIR-NDC. It is shown that the proposed stochastic ANN-PSOSQP procedure is precisely based on the AE for the SEIR-NDC.

Figure 5 presents the statistical performances using the MSE and TIC operators to solve the mathematical model. The MSE measures for the SEIR-NDC model are found as 10^{-08}–10^{-10}, 10^{-09}–10^{-10}, 10^{-07}–10^{-08}, 10^{-08}–10^{-09},

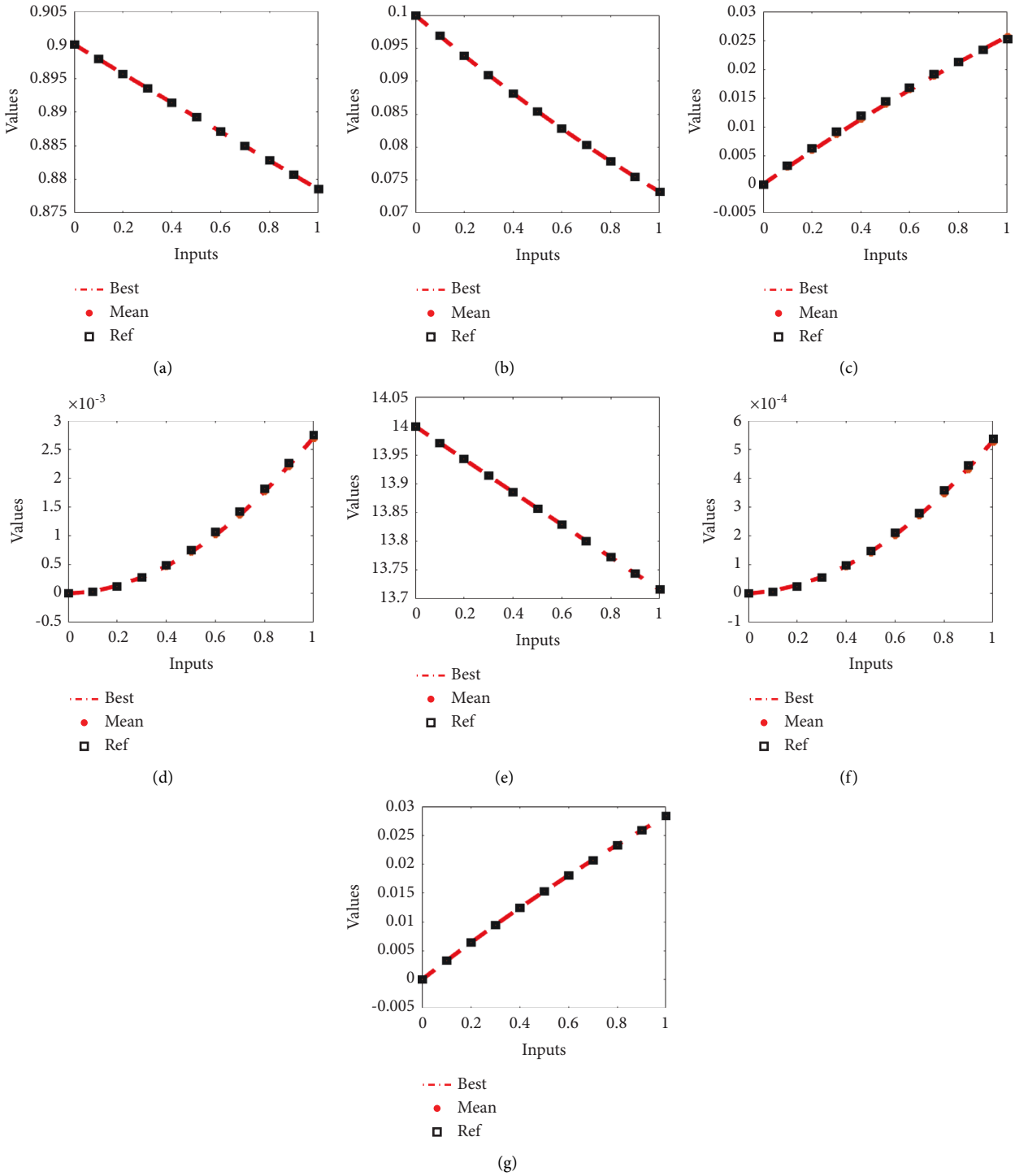

FIGURE 3: Comparison of the mean, exact, and best results for the mathematical SEIR-NDC system. (a) Result comparison of $\widehat{S}(y)$. (b) Result comparison of $\widehat{E}(y)$. (c) Result comparison of $\widehat{I}(y)$. (d) Result comparison of $\widehat{R}(y)$. (e) Result comparison of $\widehat{N}(y)$. (f) Result comparison of $\widehat{D}(y)$. (g) Result comparison of $\widehat{C}(y)$.

10^{-11}–10^{-12}, 10^{-09}–10^{-10}, and 10^{-10}–10^{-12} for each dynamics of the model. The TIC performance for the SEIR-NDC model are found around 10^{-06}–10^{-08}, 10^{-07}–10^{-08}, 10^{-03}–10^{-04}, 10^{-04}–10^{-05}, 10^{-12}–10^{-13}, 10^{-04}–10^{-05}, and 10^{-08}–10^{-10} for respective dynamics of the system. These optimal small performances enhance the value and correctness of proposed stochastic ANN-PSOSQP procedure.

Figure 6 shows the convergence study based on the MSE and TIC operators. It was noted that most of the runs resulted in a high level of fitness. Based on these analyses, it is

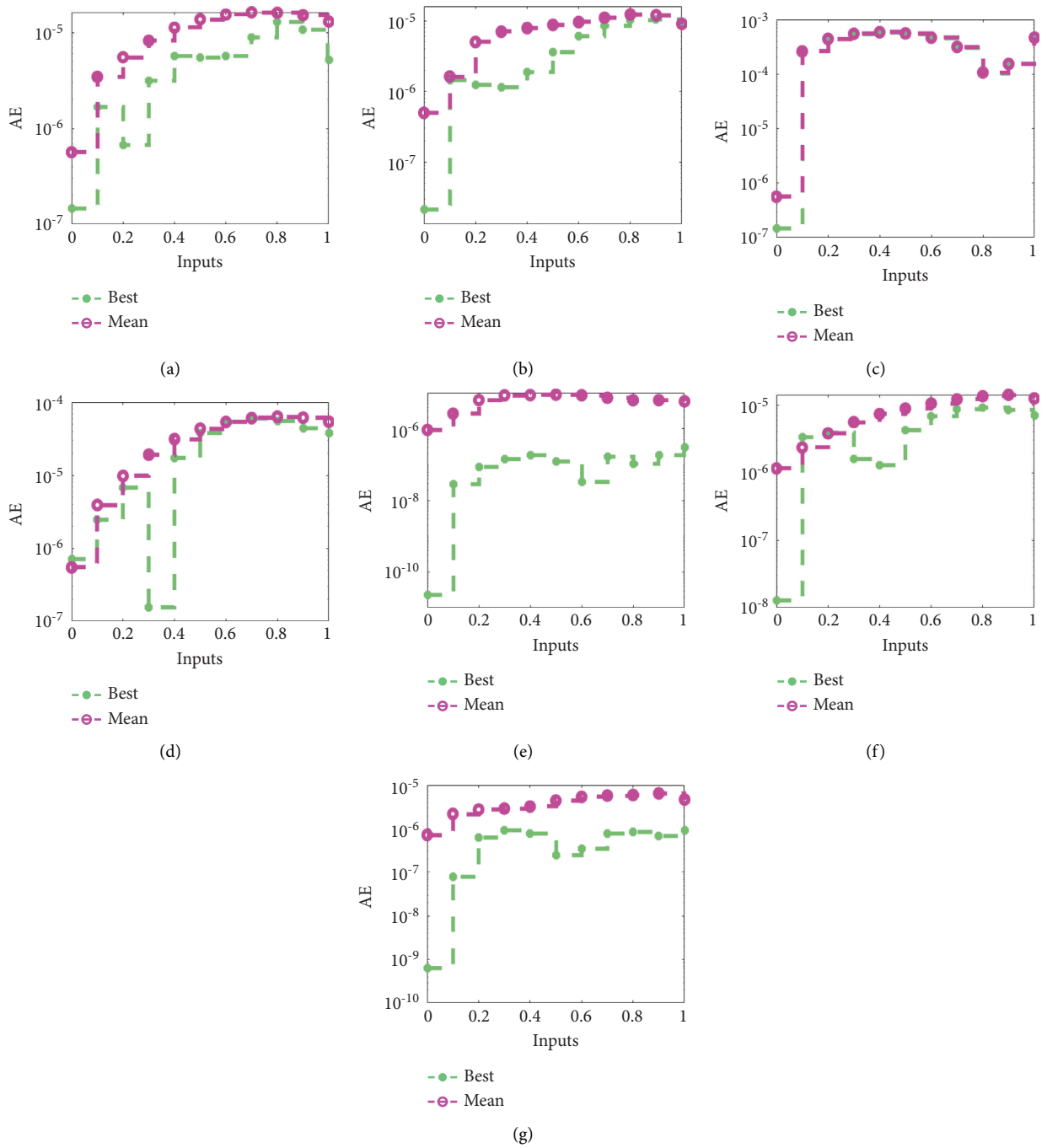

FIGURE 4: AE using the mean and best results for the nonlinear system. (a) AE performances for $\widehat{S}(y)$. (b) AE performances for $\widehat{E}(y)$. (c) AE performances for $\widehat{I}(y)$. (d) AE performances for $\widehat{R}(y)$. (e) AE performances for $\widehat{N}(y)$. (f) AE performances for $\widehat{D}(y)$. (g) AE performances for $\widehat{C}(y)$.

shown that most of the executions produced higher fitness levels that proves the procedure is reliable and stable.

Tables 2–8 provide the correctness, precision, and accurateness of the designed ANN-PSOSQP approach based on the statistical representations of the classes $\widehat{S}(y)$, $\widehat{I}(y)\widehat{R}(y)$, $\widehat{N}(y)$, $\widehat{D}(y)$, and $\widehat{C}(y)$ of the SEIR-NDC mathematical system. The statistical illustrations are presented for the maximum (Max), semi-interquartile range (SIR), minimum (Min), standard deviation (SD), mean, and median (MD) operators. The Max and Min operators specify the worst and best runs. The Max values based on the worst runs lie as 10^{-04} to 10^{-06} for the classes. The statistical Min operator values performed were found as 10^{-06}–10^{-13}, 10^{-07}–10^{-10}, 10^{-05}–10^{-12}, 10^{-05}–10^{-10}, 10^{-07}–10^{-11}, 10^{-06}–10^{-11}, and 10^{-07}–10^{-11} for each dynamics of the system. The SIR, MD, mean, and SD statistical values lie around 10^{-06}–10^{-09} of each dynamics of the model. These statistical performances present the

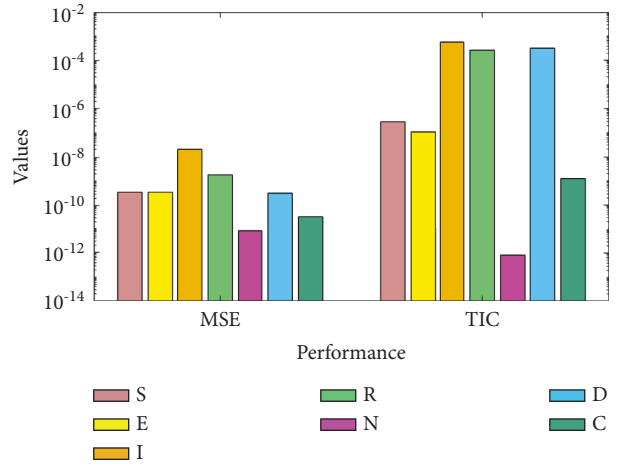

Figure 5: Statistical performances for the mathematical SEIR-NDC system.

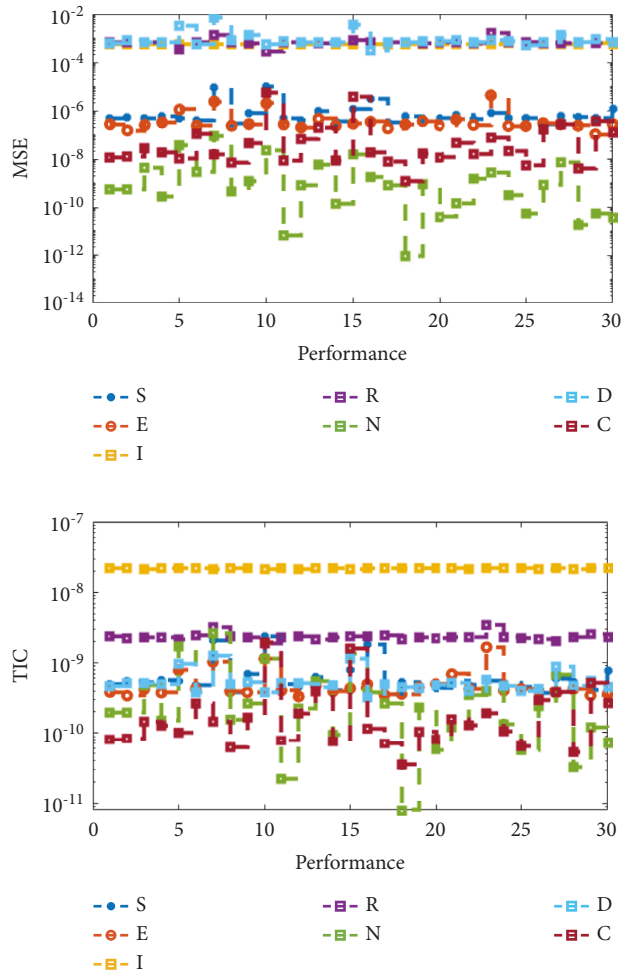

Figure 6: MSE and TIC convergence plots for the mathematical SEIR-NDC system.

Table 2: Statistical performances for the class $S(y)$ of the model.

y	$S(y)$					
	Max	SIR	Min	SD	Mean	MD
0	4.14847E-07	2.45733E-07	4.77285E-13	9.72224E-07	5.65438E-07	1.61416E-07
0.1	3.43018E-05	1.35393E-06	4.75690E-08	7.41284E-06	3.45398E-06	1.47969E-06
0.2	4.35970E-05	1.56468E-06	6.72517E-07	8.38919E-06	5.53205E-06	3.15588E-06
0.3	5.48928E-05	1.75403E-06	6.36321E-07	1.06886E-05	8.22091E-06	5.54958E-06
0.4	6.04801E-05	2.10799E-06	1.52531E-06	1.27852E-05	1.12576E-05	6.80979E-06
0.5	6.10558E-05	2.00471E-06	4.91716E-06	1.32654E-05	1.37476E-05	8.76556E-06
0.6	5.71444E-05	1.72297E-06	5.65694E-06	1.25290E-05	1.54038E-05	1.17188E-05
0.7	5.73368E-05	2.59359E-06	7.15833E-06	1.11478E-05	1.62769E-05	1.29955E-05
0.8	5.28638E-05	2.15910E-06	6.92380E-06	9.13535E-06	1.60719E-05	1.30170E-05
0.9	4.29129E-05	1.66618E-06	7.26516E-06	7.99805E-06	1.51653E-05	1.26148E-05
1	4.59409E-05	8.96879E-07	3.19198E-06	7.32537E-06	1.30260E-05	1.16572E-05

Table 3: Statistical performances for the class $E(y)$ to solve the mathematical SEIR-NDC system.

y	$E(y)$					
	Max	SIR	Min	SD	Mean	MD
0	4.75086E-06	2.96939E-07	9.83620E-10	9.46658E-07	4.96867E-07	9.25922E-08
0.1	1.28771E-05	5.14479E-07	2.09799E-08	2.87660E-06	1.62623E-06	6.62741E-07
0.2	3.46180E-05	1.59348E-06	1.58369E-07	8.31965E-06	5.00211E-06	1.88446E-06
0.3	5.05547E-05	1.76810E-06	5.24284E-07	1.10046E-05	7.01565E-06	3.36419E-06
0.4	5.27680E-05	1.93202E-06	4.44707E-07	1.03637E-05	7.89142E-06	5.38967E-06
0.5	3.68427E-05	2.42961E-06	5.06646E-07	7.47919E-06	8.75240E-06	7.61206E-06
0.6	3.24343E-05	1.28777E-06	2.93991E-07	4.97252E-06	9.60879E-06	9.24771E-06
0.7	3.30130E-05	1.08012E-06	3.30355E-06	4.76950E-06	1.10794E-05	1.04494E-05
0.8	3.35403E-05	1.07412E-06	2.26763E-06	6.10328E-06	1.23142E-05	1.12846E-05
0.9	3.35538E-05	1.54209E-06	5.45111E-07	6.27136E-06	1.19936E-05	1.06522E-05
1	2.19173E-05	9.50185E-07	2.27305E-08	3.62661E-06	9.06845E-06	9.08091E-06

Table 4: Statistical performances for the class $I(y)$ to solve the mathematical SEIR-NDC system.

y	$I(y)$					
	Max	SIR	Min	SD	Mean	MD
0	5.41754E-06	2.75761E-07	3.72458E-12	1.17847E-06	5.61374E-07	1.36275E-07
0.1	2.75677E-04	1.28020E-06	2.53537E-04	4.11470E-06	2.59946E-04	2.59379E-04
0.2	4.55826E-04	1.39173E-06	4.31680E-04	4.66773E-06	4.40432E-04	4.40370E-04
0.3	5.58989E-04	2.08120E-06	5.34904E-04	5.08382E-06	5.47084E-04	5.47243E-04
0.4	5.94001E-04	1.23786E-06	5.67049E-04	6.05079E-06	5.84125E-04	5.84972E-04
0.5	5.68161E-04	2.76336E-06	5.36930E-04	7.14524E-06	5.55266E-04	5.56218E-04
0.6	4.84700E-04	2.47091E-06	4.44792E-04	8.47217E-06	4.63991E-04	4.64920E-04
0.7	3.39830E-04	1.73645E-06	2.94297E-04	9.89722E-06	3.13563E-04	3.13775E-04
0.8	1.34826E-04	1.87554E-06	8.57211E-05	1.07004E-05	1.06965E-04	1.06549E-04
0.9	1.74484E-04	1.13857E-06	1.28803E-04	9.96170E-06	1.53142E-04	1.53830E-04
1	4.90050E-04	1.01315E-06	4.51017E-04	7.32199E-06	4.64416E-04	4.64311E-04

Table 5: Statistical performances for the class $R(y)$ to solve the mathematical SEIR-NDC system.

y	$R(y)$					
	Max	SIR	Min	SD	Mean	MD
0	3.41437E-05	2.37597E-07	2.34978E-10	9.85762E-07	5.45699E-07	1.29018E-07
0.1	1.18197E-04	1.13076E-06	4.57222E-07	2.72914E-06	3.90519E-06	3.00401E-06
0.2	1.94783E-04	1.31799E-06	1.68986E-06	4.15290E-06	9.76711E-06	9.79606E-06
0.3	3.11757E-04	2.95319E-06	1.55537E-07	5.99365E-06	1.90733E-05	1.95954E-05
0.4	4.12688E-04	3.13432E-06	1.72611E-05	5.37846E-06	3.11529E-05	3.13887E-05
0.5	6.15166E-04	3.31077E-06	3.30247E-05	6.07381E-06	4.31572E-05	4.27264E-05
0.6	8.09984E-05	1.96736E-06	4.47792E-05	7.79507E-06	5.33325E-05	5.19418E-05
0.7	9.38333E-05	1.84372E-06	4.38602E-05	9.07666E-06	6.03332E-05	5.89380E-05
0.8	9.77846E-05	7.95787E-07	4.05124E-05	9.75804E-06	6.31963E-05	6.27128E-05
0.9	9.12796E-05	2.02403E-06	3.79806E-05	9.65600E-06	6.12207E-05	6.10542E-05
1	7.33207E-05	9.80744E-07	3.80090E-05	6.72537E-06	5.38149E-05	5.40220E-05

Table 6: Statistical performances for the class $N(y)$ to solve the mathematical SEIR-NDC system.

y	$N(y)$					
	Max	SIR	Min	SD	Mean	MD
0	9.65096E-05	3.16692E-07	2.32632E-11	1.93612E-06	9.21061E-07	2.73802E-07
0.1	2.18383E-05	1.02040E-06	2.76323E-08	4.15033E-06	2.61757E-06	1.70645E-06
0.2	2.76927E-05	3.08333E-06	7.57758E-08	6.90415E-06	6.25072E-06	3.82658E-06
0.3	3.96641E-05	3.99790E-06	7.15828E-09	9.78686E-06	8.47392E-06	4.29770E-06
0.4	4.95862E-05	5.51404E-06	1.25805E-07	1.20188E-05	8.60042E-06	3.68434E-06
0.5	5.11064E-05	6.05062E-06	5.79059E-09	1.24962E-05	8.84438E-06	2.22204E-06
0.6	5.30185E-05	4.70764E-06	7.41051E-09	1.31610E-05	8.51820E-06	4.00156E-06
0.7	7.28155E-05	2.57856E-06	1.63822E-07	1.46255E-05	7.24511E-06	2.27404E-06
0.8	8.19951E-05	1.53702E-06	4.43392E-08	1.54233E-05	6.19774E-06	2.04275E-06
0.9	7.54090E-05	2.01301E-06	1.02477E-07	1.40382E-05	6.21569E-06	2.59263E-06
1	4.79690E-05	1.98560E-06	4.90144E-08	1.02712E-05	5.75728E-06	2.06130E-06

Table 7: Statistical performances for the class $D(y)$ to solve the mathematical SEIR-NDC system.

y	$D(y)$					
	Max	SIR	Min	SD	Mean	MD
0	2.55036E-05	2.42996E-07	1.20788E-11	4.62219E-06	1.15625E-06	1.05220E-07
0.1	1.84948E-05	9.71835E-07	4.59191E-08	4.10983E-06	2.36323E-06	9.52892E-07
0.2	1.77093E-05	1.26636E-06	1.68545E-07	4.13578E-06	3.82845E-06	2.47213E-06
0.3	1.88607E-05	1.70762E-06	4.08993E-07	4.28106E-06	5.61650E-06	4.59504E-06
0.4	2.64931E-05	1.55731E-06	1.28199E-06	5.09365E-06	7.41478E-06	6.54103E-06
0.5	3.03275E-05	2.01054E-06	5.69120E-07	5.35037E-06	8.93916E-06	8.43291E-06
0.6	2.81061E-05	1.74536E-06	1.29764E-06	4.75049E-06	1.06058E-05	1.02894E-05
0.7	3.14862E-05	1.60627E-06	3.06673E-06	4.88070E-06	1.22384E-05	1.17988E-05
0.8	4.09111E-05	7.70645E-07	9.81581E-07	6.41026E-06	1.35938E-05	1.26136E-05
0.9	4.21191E-05	1.73597E-06	5.17936E-06	7.19353E-06	1.42641E-05	1.25719E-05
1	3.50801E-05	1.30583E-06	2.03979E-06	6.07739E-06	1.26104E-05	1.12803E-05

Table 8: Statistical performances for the class $C(y)$ to solve the mathematical SEIR-NDC system.

y	$C(y)$					
	Max	SIR	Min	SD	Mean	MD
0	7.76923E-06	1.99620E-07	3.87874E-11	1.76960E-06	7.18293E-07	1.16157E-07
0.1	1.43901E-05	6.81331E-07	3.83744E-08	3.66051E-06	2.17221E-06	8.58069E-07
0.2	1.75513E-05	1.10384E-06	6.95938E-08	4.42693E-06	2.73246E-06	1.12893E-06
0.3	1.54017E-05	1.17901E-06	2.12959E-07	3.28945E-06	2.87969E-06	1.63906E-06
0.4	1.28635E-05	2.11604E-06	8.01746E-08	3.48020E-06	3.21899E-06	1.66457E-06
0.5	2.70540E-05	2.87815E-06	1.90426E-08	5.80604E-06	4.39566E-06	1.79130E-06
0.6	4.36450E-05	2.43142E-06	6.15750E-09	9.11304E-06	5.35181E-06	2.75264E-06
0.7	5.57509E-05	1.44891E-06	3.58756E-07	1.23557E-05	5.72802E-06	2.31043E-06
0.8	6.04390E-05	1.19585E-06	4.22483E-08	1.41987E-05	5.91669E-06	1.74317E-06
0.9	5.51061E-05	1.26357E-06	6.25928E-08	1.29102E-05	6.43255E-06	2.76458E-06
1	3.74735E-05	1.27784E-06	1.29893E-07	7.96444E-06	4.65701E-06	2.25638E-06

consistency and trustworthiness of the designed ANN-PSOSQP.

4. Concluding Remarks

The current work obtains the numerical solutions of the coronavirus mathematical system using the computational structure of artificial neural networks, swarming optimization procedures, and the sequential quadratic programming. The particle swarm optimization works as a global swarming procedure, whereas the sequential quadratic programming is implemented as a local search algorithm approach. The optimization of the cost function which is constructed using the mathematical SEIR-NDC system is performed through the stochastic swarming procedures. The correctness of the stochastic ANN-PSOSQP computing scheme has been verified through the comparison of the obtained performances of the mathematical SEIR-NDC system and the Runge–Kutta scheme. The statistical MSE and TIC operators have been provided in good ranges for 10 neurons or 30 variables for the mathematical SEIR-NDC system. The negligible statistical Max, Min, SIR, SD, mean,

and MD operator values show the accuracy. Moreover, the graphical illustrations of the performance indices, absolute error, and convergence curves have been derived to validate the robustness of the proposed ANN-PSOSQP approach for the mathematical SEIR-NDC system. These statistical operator performances authenticate that the proposed ANN-PSOSQP approach is stable, reliable, accurate, and robust for the numerical solutions of the mathematical SEIR-NDC system.

The proposed stochastic paradigms can be explored in the future to present the numerical solutions of the nonlinear mathematical systems [52–61].

Data Availability

No data were used to support this study.

Conflicts of Interest

The authors declare that they have no conflicts of interest.

Authors' Contributions

All authors contributed equally and significantly in writing this paper. All authors read and approved the final manuscript.

Acknowledgments

This research was supported by Chiang Mai University and the NSRF via the Program Management Unit for Human Resources and Institutional Development, Research and Innovation (grant no. B05F640183). Watcharaporn Cholamjiak would like to thank National Research Council of Thailand (N42A650334) and Thailand Science Research and Innovation, the University of Phayao (FF66-UoE).

References

[1] V. K. Ramani, R. Shinduja, K. P. Suresh, and R. Naik, "A study on the global scenario of COVID-19 related case fatality rate, recovery rate and prevalence rate and its implications for India—a record based retrospective cohort study," *Advances in Infectious Diseases*, vol. 10, no. 03, pp. 233–248, 2020.

[2] W. D. Strain, O. Sherwood, A. Banerjee, V. Van der Togt, L. Hishmeh, and J. Rossman, "The impact of COVID vaccination on symptoms of long COVID: an international survey of people with lived experience of long COVID," *Vaccines*, vol. 10, no. 5, p. 652, 2022.

[3] A. Atangana, "Modelling the spread of COVID-19 with new fractal-fractional operators: can the lockdown save mankind before vaccination?" *Chaos, Solitons & Fractals*, vol. 136, Article ID 109860, 2020.

[4] C. D. Pratiwi and S. Mungkasi, "Euler's and Heun's numerical solutions to a mathematical model of the spread of COVID-19," in *AIP Conference Proceedings*, vol. 2353, no. 1, 2021 May, Article ID 030110.

[5] E. Atangana and A. Atangana, "Facemasks simple but powerful weapons to protect against COVID-19 spread: can they have sides effects?" *Results in Physics*, vol. 19, Article ID 103425, 2020.

[6] M. A. Khan and A. Atangana, "Mathematical modeling and analysis of COVID-19: a study of new variant Omicron," *Physica A: Statistical Mechanics and Its Applications*, vol. 599, Article ID 127452, 2022.

[7] J. Wang, "Mathematical models for COVID-19: applications, limitations, and potentials," *Journal of Public Health and Epidemiology*, vol. 4, p. 9, 2020.

[8] F. Donders, R. Lonnee-Hoffmann, A. Tsiakalos et al., "ISIDOG recommendations concerning COVID-19 and pregnancy," *Diagnostics*, vol. 10, no. 4, p. 243, 2020.

[9] T. Rhodes and K. Lancaster, "Mathematical models as public troubles in COVID-19 infection control: following the numbers," *Health Sociology Review*, vol. 29, no. 2, pp. 177–194, 2020.

[10] P. Khrapov and A. Loginova, "Comparative analysis of the mathematical models of the dynamics of the coronavirus COVID-19 epidemic development in the different countries," *International Journal of Open Information Technologies*, vol. 8, no. 5, pp. 17–22, 2020.

[11] B. L. Jewell, E. Mudimu, J. Stover et al., "Potential effects of disruption to HIV programmes in sub-Saharan Africa caused by COVID-19: results from multiple mathematical models," *The Lancet HIV*, vol. 7, no. 9, pp. e629–e640, 2020.

[12] Y. G. Sánchez, Z. Sabir, and J. L. G. Guirao, "Design of a nonlinear SITR fractal model based on the dynamics of a novel coronavirus (COVID-19)," *Fractals*, vol. 28, no. 08, Article ID 2040026, 2020.

[13] R. N. Thompson, "Epidemiological models are important tools for guiding COVID-19 interventions," *BMC Medicine*, vol. 18, pp. 152–154, 2020.

[14] A. Elsonbaty, U. Sabir, R. Ramaswamy, and W. Adel, "Dynamical analysis of a novel discrete fractional SITRs model for COVID-19," *Fractals*, vol. 29, Article ID 2140035, 2021.

[15] M. Umar, Z. Sabir, M. A. Z. Raja, M. Shoaib, M. Gupta, and Y. G. Sanchez, "A stochastic intelligent computing with neuro-evolution heuristics for nonlinear SITR system of novel COVID-19 dynamics," *Symmetry*, vol. 12, no. 10, p. 1628, 2020.

[16] M. Umar, Z. Sabir, M. A. Z. Raja, F. Amin, T. Saeed, and Y. Guerrero-Sanchez, "Integrated neuro-swarm heuristic with interior-point for nonlinear SITR model for dynamics of novel COVID-19," *Alexandria Engineering Journal*, vol. 60, no. 3, pp. 2811–2824, 2021.

[17] A. Shikongo, S. M. Nuugulu, D. Elago, A. T. Salom, and K. M. Owolabi, "Fractional derivative operator on quarantine and isolation principle for COVID-19," in *Advanced Numerical Methods for Differential Equations*, pp. 205–226, CRC Press, Boca Raton, NY, USA, 2021.

[18] S. Side, R. Yulita Molliq, P. Dian Gerhana, and Marlina, "Stability analysis susceptible, exposed, infected, recovered (SEIR) model for spread of dengue fever in medan," *Statistics, Mathematics, Teaching, and Research*, vol. 246, 2015.

[19] K. M. Owolabi, K. C Patidar, and A. Shikongo, "Efficient numerical method for a model arising in biological stoichiometry of tumour dynamics," *Discrete & Continuous Dynamical Systems-S*, vol. 12, no. 3, pp. 591–613, 2019.

[20] K. M. Owolabi, K. C. Patidar, and A. Shikongo, "A fitted numerical method for a model arising in HIV related cancer-immune system dynamics," *Communications Now*, vol. 2019, 2019.

[21] K. M. Owolabi and A. Shikongo, "Fractional operator method on a multi-mutation and intrinsic resistance model," *Alexandria Engineering Journal*, vol. 59, no. 4, pp. 1999–2013, 2020.

[22] M. Umar, Z. Sabir, and M. A. Z. Raja, "Intelligent computing for numerical treatment of nonlinear prey–predator models," *Applied Soft Computing*, vol. 80, pp. 506–524, 2019.

[23] Z. Sabir, J. L. Guirao, and T. Saeed, "Solving a novel designed second order nonlinear Lane–Emden delay differential model using the heuristic techniques," *Applied Soft Computing*, vol. 102, Article ID 107105, 2021.

[24] J. L. Guirao, Z. Sabir, and T. Saeed, "Design and numerical solutions of a novel third-order nonlinear Emden–Fowler delay differential model," *Mathematical Problems in Engineering*, vol. 2020, pp. 1–9, Article ID 7359242, 2020.

[25] Z. Sabir, M. Asif Zahoor Raja, J. L. Guirao, and M. Shoaib, "A novel design of fractional Meyer wavelet neural networks with application to the nonlinear singular fractional Lane-Emden systems," *Alexandria Engineering Journal*, vol. 60, no. 2, pp. 2641–2659, 2021.

[26] Z. Sabir, M. A. Zahoor Raja, and D. Baleanu, "Fractional Mayer Neuro-swarm heuristic solver for multi-fractional Order doubly singular model based on Lane-Emden equation," Fractals, 2021.

[27] Z. Sabir, M. A. Z. Raja, M. Shoaib, and J. F. G. Aguilar, "FMNEICS: fractional Meyer neuro-evolution-based intelligent computing solver for doubly singular multi-fractional order Lane–Emden system," *Computational and Applied Mathematics*, vol. 39, no. 4, pp. 303–318, 2020.

[28] Z. Sabir, C. M. Khalique, M. A. Z. Raja, and D. Baleanu, "Evolutionary computing for nonlinear singular boundary value problems using neural network, genetic algorithm and active-set algorithm," *The European Physical Journal Plus*, vol. 136, no. 2, pp. 1–19, 2021.

[29] Z. Sabir, M. A. Z. Raja, J. L. G. Guirao, and M. Shoaib, "A neuro-swarming intelligence-based computing for second order singular periodic non-linear boundary value problems," *Frontiers in Physiology*, vol. 8, p. 224, 2020.

[30] I. Ahmad, S. Ahmad, M. Awais, S. Ul Islam Ahmad, and M. Asif Zahoor Raja, "Neuro-evolutionary computing paradigm for Painlevé equation-II in nonlinear optics," *The European Physical Journal Plus*, vol. 133, no. 5, p. 184, 2018.

[31] M. Umar, Z. Sabir, F. Amin, J. L. G. Guirao, and M. A. Z. Raja, "Stochastic numerical technique for solving HIV infection model of CD4+ T cells," *The European Physical Journal Plus*, vol. 135, no. 5, p. 403, 2020.

[32] M. Umar, F. Amin, H. A. Wahab, and D. Baleanu, "Unsupervised constrained neural network modeling of boundary value corneal model for eye surgery," *Applied Soft Computing*, vol. 85, Article ID 105826, 2019.

[33] B. Wang, J. F. Gomez-Aguilar, Z. Sabir et al., "Numerical computing to solve the nonlinear corneal system of eye surgery using the capability of Morlet wavelet artificial neural networks," *Fractals*, vol. 30, no. 05, 2022.

[34] Z. Sabir, M. A. Z. Raja, M. Umar, and M. Shoaib, "Neuro-swarm intelligent computing to solve the second-order singular functional differential model," *The European Physical Journal Plus*, vol. 135, no. 6, p. 474, 2020.

[35] M. Umar, M. A. Z. Raja, Z. Sabir, A. S. Alwabli, and M. Shoaib, "A stochastic computational intelligent solver for numerical treatment of mosquito dispersal model in a heterogeneous environment," *The European Physical Journal Plus*, vol. 135, no. 7, pp. 1–23, 2020.

[36] Z. Sabir, M. A. Manzar, M. A. Z. Raja, M. Sheraz, and A. M. Wazwaz, "Neuro-heuristics for nonlinear singular Thomas-Fermi systems," *Applied Soft Computing*, vol. 65, pp. 152–169, 2018.

[37] T. Saeed, Z. Sabir, M. Alhodaly, H. H. Alsulami, and Y. Guerrero Sanchez, "An advanced heuristic approach for a nonlinear mathematical based medical smoking model," *Results in Physics*, vol. 32, Article ID 105137, 2022.

[38] Z. Sabir, "Stochastic numerical investigations for nonlinear three-species food chain system," *International Journal of Biomathematics*, vol. 15, no. 04, Article ID 2250005, 2022.

[39] F. Wang, H. Zhang, and A. Zhou, "A particle swarm optimization algorithm for mixed-variable optimization problems," *Swarm and Evolutionary Computation*, vol. 60, Article ID 100808, 2021.

[40] A. H. Elsheikh and M. Abd Elaziz, "Review on applications of particle swarm optimization in solar energy systems," *International journal of Environmental Science and Technology*, vol. 16, no. 2, pp. 1159–1170, 2019.

[41] A. Darwish, D. Ezzat, and A. E. Hassanien, "An optimized model based on convolutional neural networks and orthogonal learning particle swarm optimization algorithm for plant diseases diagnosis," *Swarm and Evolutionary Computation*, vol. 52, Article ID 100616, 2020.

[42] Y. Xue, B. Xue, and M. Zhang, "Self-adaptive particle swarm optimization for large-scale feature selection in classification," *ACM Transactions on Knowledge Discovery from Data*, vol. 13, no. 5, pp. 1–27, 2019.

[43] D. Yousri, S. B. Thanikanti, D. Allam, V. K. Ramachandaramurthy, and M. B. Eteiba, "Fractional chaotic ensemble particle swarm optimizer for identifying the single, double, and three diode photovoltaic models' parameters," *Energy*, vol. 195, Article ID 116979, 2020.

[44] H. Chen, D. L. Fan, L. Fang et al., "Particle swarm optimization algorithm with mutation operator for particle filter noise reduction in mechanical fault diagnosis," *International Journal of Pattern Recognition and Artificial Intelligence*, vol. 34, no. 10, Article ID 2058012, 2020.

[45] H. Fu, Z. Li, Z. Liu, and Z. Wang, "Research on big data digging of hot topics about recycled water use on micro-blog based on particle swarm optimization," *Sustainability*, vol. 10, no. 7, p. 2488, 2018.

[46] Z. Cui, J. Zhang, D. Wu et al., "Hybrid many-objective particle swarm optimization algorithm for green coal production problem," *Information Sciences*, vol. 518, pp. 256–271, 2020.

[47] S. Sivasubramani and K. S. Swarup, "Sequential quadratic programming based differential evolution algorithm for optimal power flow problem," *IET Generation, Transmission & Distribution*, vol. 5, no. 11, pp. 1149–1154, 2011.

[48] M. Basu, "Hybridization of bee colony optimization and sequential quadratic programming for dynamic economic dispatch," *International Journal of Electrical Power & Energy Systems*, vol. 44, no. 1, pp. 591–596, 2013.

[49] T. A. Johansen, T. I. Fossen, and S. P. Berge, "Constrained nonlinear control allocation with singularity avoidance using sequential quadratic programming," *IEEE Transactions on Control Systems Technology*, vol. 12, no. 1, pp. 211–216, 2004.

[50] A. Gharaei and S. H. R. Pasandideh, "Modeling and optimization of four-level integrated supply chain with the aim of determining the optimum stockpile and period length: sequential quadratic programming," *Journal of Industrial and Production Engineering*, vol. 34, no. 7, pp. 529–541, 2017.

[51] X. Lin, Z. Wang, S. Zeng, W. Huang, and X. Li, "Real-time optimization strategy by using sequence quadratic programming with multivariate nonlinear regression for a fuel cell electric vehicle," *International Journal of Hydrogen Energy*, vol. 46, no. 24, pp. 13240–13251, 2021.

[52] K. A. Abro and A. Atangana, "Numerical and mathematical analysis of induction motor by means of AB–fractal–fractional differentiation actuated by drilling system," *Numerical Methods for Partial Differential Equations*, vol. 38, no. 3, pp. 293–307, 2022.

[53] K. A. Abro and A. Atangana, "Dual fractional modeling of rate type fluid through non-local differentiation," *Numerical Methods for Partial Differential Equations*, vol. 38, no. 3, pp. 390–405, 2022.

[54] A. Atangana and A. Akgül, "On solutions of fractal fractional differential equations," *Discrete & Continuous Dynamical Systems-S*, vol. 14, no. 10, p. 3441, 2021.

[55] K. A. Abro and A. Atangana, "Strange attractors and optimal analysis of chaotic systems based on fractal verses fractional differential operators," *International Journal of Modelling and Simulation*, vol. 42, no. 5, pp. 716–724, 2021.

[56] A. Atangana, "Mathematical model of survival of fractional calculus, critics and their impact: how singular is our world?" *Advances in Difference Equations*, vol. 2021, no. 1, pp. 403–459, 2021.

[57] A. Atangana and S. I. araz, "A novel Covid-19 model with fractional differential operators with singular and non-singular kernels: analysis and numerical scheme based on Newton polynomial," *Alexandria Engineering Journal*, vol. 60, no. 4, pp. 3781–3806, 2021.

[58] R. Chaharpashlou, A. Atangana, and R. Saadati, "On the fuzzy stability results for fractional stochastic Volterra integral equation," *Discrete & Continuous Dynamical Systems-S*, vol. 14, no. 10, p. 3529, 2021.

[59] M. Shoaib, G. Zubair, K. S. Nisar et al., "Ohmic heating effects and entropy generation for nanofluidic system of Ree-Eyring fluid: intelligent computing paradigm," *International Communications in Heat and Mass Transfer*, vol. 129, Article ID 105683, 2021.

[60] M. A. Z. Raja, M. Shoaib, S. Hussain, K. S. Nisar, and S. Islam, "Computational intelligence of Levenberg-Marquardt back-propagation neural networks to study thermal radiation and Hall effects on boundary layer flow past a stretching sheet," *International Communications in Heat and Mass Transfer*, vol. 130, Article ID 105799, 2022.

[61] Z. I. Butt, I. Ahmad, M. Shoaib, H. Ilyas, and M. A. Z. Raja, "Electro-magnetohydrodynamic impact on Darrcy-Forchheimer viscous fluid flow over a stretchable surface: integrated intelligent Neuro-evolutionary computing approach," *International Communications in Heat and Mass Transfer*, vol. 137, Article ID 106262, 2022.